An Application of Neural Network-based Sliding Mode Control for Multilevel Inverters

Quang-Tho Tran
Faculty of Electrical and Electronics Engineering, HCMC University of Technology and Education, Vietnam
thotq@hcmute.edu.vn (corresponding author)

Received: 13 October 2023 | Revised: 30 October 2023 | Accepted: 15 November 2023

 HTTPS://DOI.ORG/https://doi.org/10.48084/etasr.6516

ABSTRACT

Multi-level 3-phase inverters using cascaded H-bridges are becoming prominent in the electric drive and renewable energy sectors due to their high capacity and ability to withstand high voltage shocks. Therefore, the modulation and control techniques used in these multilevel inverters have a crucial influence on the quality of the output voltage they produce. The significantly high common-mode voltage amplitude they generate is one of their disadvantages, causing leakage currents and harmonics. This article proposes a new technique using sliding mode control combined with neural networks to manage a three-phase multi-level inverter. The research objective of this innovative technique is to eliminate the need for current controllers and conventional modulation that relies on carrier signals, reducing hardware calculations and enhancing dynamic response. In addition, it demonstrates the ability to minimize harmonics, common mode voltage, and the number of switching counts, thereby limiting the inverter switching losses and increasing device performance. Simulation results performed on a 5-level 3-phase inverter using cascaded H-bridges have confirmed the effectiveness of the proposed method.

Keywords-multilevel inverter; common mode voltage; neural network controller; phase opposition disposition

I. INTRODUCTION

Multilevel Inverters (MLIs) have gained significant attention in the realm of industrial applications and electric vehicles [1-5]. This interest arose because 2-level inverters often grapple with limitations imposed by semiconductor blocking voltages when attempting to match grid voltage ranges. As a result, MLIs have emerged as the preferred choice for grid interfacing. They not only mitigate the high voltage shock on power switching transistors, but also reduce voltage Total Harmonic Distortion (THD) to align with the power grid regulations. Furthermore, they exhibit a propensity for reduced power dissipation in semiconductor switches and diminished electromagnetic interference. Traditionally, MLIs are divided into three primary topological categories: Cascaded H-Bridges (CHBs), flying capacitor MLIs, and neutral point clamped MLIs. CHB configurations enjoy widespread use due to their modular adaptability, which can effortlessly accommodate varying levels. Numerous studies have concentrated on adapting conventional voltage source inverters to control multilevel strategies [6]. Simultaneously, research has delved into exploring modulation techniques to optimize MLI performance across various configurations. These modulation techniques are typically classified based on their switching frequency range. High-frequency modulation techniques are constrained, as they can degrade inverter ratings and overall efficiency due to increased switching losses. One commonly employed technique is Sinusoidal Pulse-Width Modulation (SPWM) based on phase-shifted carriers, favored for industrial applications because of its minimal harmonic content in the output voltage waveform. Another widely adopted method is space vector modulation [7], known for its exceptional performance in 3-level topologies. Modulation techniques of low switching frequency, such as space-vector control, selective harmonic elimination, and staircase modulation, have gained prominence and found utility across a broad spectrum of applications.

Common Mode Voltage (CMV) in the cascaded 3-phase MLIs emerges as a critical factor necessitating attention. The significant CMV magnitude exerts adverse effects on the performance of 3-phase induction motors, manifesting as leakage currents and high-frequency noises [8, 9]. In grid-connected systems using MLIs, particularly those driven by renewable energy sources, the CMV exacerbates the issue by giving rise to leakage currents and introducing harmonic distorted currents into the power grid [10]. Hence, a range of solutions has been explored to enhance the power quality of inverter outputs, primarily focusing on strategies to lessen common mode voltage. Nevertheless, the pursuit of reducing harmonics by increasing the carrier wave frequency brings with it challenges such as greater memory requirements and a higher switching count, consequently elevating switching losses. These considerations underscore the need for a quantitative evaluation of CMV magnitudes in multilevel inverters, an aspect that has yet to receive comprehensive attention.

Neural networks (NNs), especially the Radial Basis Function (RBF) networks [11-13], have been used in various

control fields [14-17]. The method in [16] is employed to resolve the voltage restoration problem. The techniques in [18-20] are utilized for single phase inverters. The method in [21] uses Neural Networks (NNs) to predict the velocity of electric vehicles. In [22, 23], the NNs are engaged to estimate the inertia of the virtual synchronous generator and control the generator. The neural estimators in [24, 25] are applied to approximate the upper bound of the lumped nonlinearities in the active power filter. In 3-phase MLIs, several challenges persist, including the utilization of carriers for modulation and the implementation of current controllers for regulation [26]. These factors result in a reduction in dynamic response and an increase in over-shoot or under-shoot. Sliding Mode Control (SMC) is also applied [27-29]. However, the CMV and switching counts have yet to undergo a quantitative assessment.

This paper presents a technique using Enhanced SMC (ESMC) based on NNs to control the MLIs. The method presented here eliminates the need for carrier-based modulation and completely removes the use of Proportional Resonance (PR) current controllers. Consequently, this approach contributes to the reduction of CMV magnitude and enhances dynamic response. Additionally, the outcomes achieved through this innovative technique are compared with those obtained using the conventional approach in which Phase Opposition Disposition (POD) and PR controllers are employed. The performance's validity is further affirmed through the simulation results.

II. MULTILEVEL INVERTER SYSTEM

The structure of a 5-level 3-phase inverter is described in Figure 1(a) and the main circuit of phase A is shown in Figure 1(b). In this system, the PR controller is used for managing the load currents based on the reference currents. The angular frequency ω is utilized to create the reference load current and provide for the PR controller. The controller's transfer function is given by (1):

$$G_{PR}(s)=\begin{bmatrix} K_p & \dfrac{K_i}{s^2+\omega^2} \\ \dfrac{K_i}{s^2+\omega^2} & K_p \end{bmatrix} \quad (1)$$

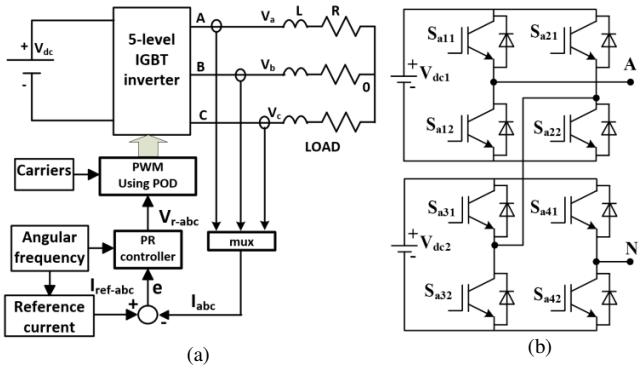

Fig. 1. Three-phase inverter system: (a) principle diagram and (b) main circuit of phase A.

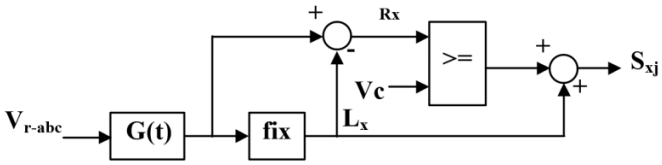

Fig. 2. Inverter control diagram.

Popular modulation methods such as Phase Disposition (PD), POD, and alternate POD (APOD) are usually employed for modulating MLIs. Although the PD method can bring THD values smaller than those of the POD and APOD, its magnitude of CMV is up to $2\times V_{dc}/3$, while the magnitude of POD or APOD is only $1\times V_{dc}/3$. Moreover, POD is simpler and more effective than the APOD method. Thus, the POD modulation method is chosen as a benchmark in this paper. In the approach outlined in [30], PWM pulses for controlling the switches are generated using the POD modulation, as illustrated in Figure 2. In this representation, S_{xj} corresponds to the ON/OFF status of the respective switches as defined in (2), with x denoting the phases a, b, and c. The top and bottom transistors of the H-bridge are symbolized as S_{xj1} and S_{xj2}, respectively. V_c is the signal of carriers.

$$S_{xj1}+S_{xj2}=1 \quad (2)$$

where j = 1, 2, 3, 4. Table I displays the configurations of transistor states for one phase of A. In this context, the level, n of 5, represents the number of levels in the inverters, and the DC source voltage values are equal. R_x and L_x represent two elements of the voltage signal $G(t)$ in the control diagram, for each phase (x = a, b, c). Here, L_x, an integer, satisfies the condition $0 \le L_x \le n-2$ within the $G(t)$ signal, and R_x, a division remainder, complies with the constraint $0 \le R_x \le 1$.

TABLE I. SWITCHING STATES FOR ONE PHASE OF A

n	S_{a11}	S_{a21}	S_{a31}	S_{a41}	Output voltage
1	1	0	1	0	$+2V_{dc}$
2	1	0	0	0	$+V_{dc}$
3	0	0	0	0	0
4	0	1	0	0	$-V_{dc}$
5	0	1	0	1	$-2V_{dc}$

III. THE PROPOSED TECHNIQUE

The presented technique structure using ESMC is illustrated in Figure 3 with the transfer function of the first-order filter being:

$$F(p)=\frac{1}{T.p+1} \quad (3)$$

where p is a derivative operator and T is the constant of time of the filter. Then, the phase voltage of load V_{r1x} is:

$$V_{r1x}=\frac{1}{T.p+1}V_f \quad (4)$$

The phase voltage of load V_{r1x} is defined as:

$$V_{r1x}=Ri_x+L\dot{i}_x \quad (5)$$

where the dot above the i_x serves as the derivative of current. Therefore, the output of SMC V_f is:

$$\begin{aligned} V_f &= V_{r1x} + T\dot{V}_{r1x} \\ &= Ri_x + L\dot{i}_x + T\left(R\dot{i}_x + L\ddot{i}_x\right) \end{aligned} \quad (6)$$

The 2nd-order derivative of the current is:

$$\ddot{i}_x = \frac{V_f - \left(L\dot{i}_x + Ri_x + TR\dot{i}_x\right)}{TL} \quad (7)$$

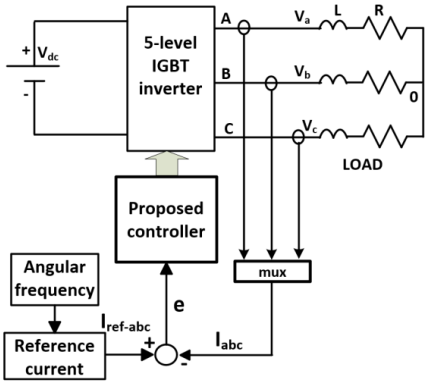

Fig. 3. Proposed control technique.

The difference between the reference value i_{refx} and the measured value of load current i_x, is the error e. The sliding surface S is chosen as:

$$S = \dot{e} + \alpha e \text{ with } \alpha > 0 \quad (8)$$

Then, we can deduce:

$$\dot{S} = \ddot{e} + \alpha\dot{e} = \ddot{i}_{refx} - \frac{\left[V_f - \left(L\dot{i}_x + Ri_x + TR\dot{i}_x\right)\right]}{TL} + \alpha\dot{e} \quad (9)$$

The chosen control law is:

$$\begin{aligned} &\dot{S} = -\beta\tanh\left(\frac{S}{\gamma}\right) - \mu S + \frac{Ri_x}{TL} + \ddot{i}_{refx} \quad \gamma, \mu > 0 \\ &\text{with } \beta > \left|\frac{Ri_x}{TL} + \ddot{i}_{refx}\right| \end{aligned} \quad (10)$$

Then:

$$V_f = TL\left[\beta\tanh\left(\frac{S}{\gamma}\right) + \mu S + \alpha\dot{e}\right] + \left(RT + L^2\right)\dot{i}_x \quad (11)$$

An RBF network is used to estimate the component N_e as follows:

$$N_e = \left(RT + L^2\right)\dot{i}_x \quad (12)$$

where:

$$\dot{i}_x = \dot{i}_{refx} - \dot{e} \quad (13)$$

The structure of this network has 2 inputs, e and the derivative of e, the hidden layer has 5 neural cells, and the output is N_e. The cells of the hidden layer are defined as:

$$g\left(x\right)_i = exp\left(-\sum_{i=1}^{n}\left[\frac{\left\|x - c_i\right\|^2}{2\sigma^2}\right]\right) \quad (14)$$

Then, we can deduce:

$$\hat{N}_e = \hat{w}^T * g \quad (15)$$

Then:

$$V_f = TL\left[\beta\tanh\left(\frac{S}{\gamma}\right) + \mu S + \alpha\dot{e}\right] + \hat{N}_e \quad (16)$$

where g is the Gauss function, $\hat{w}$ is an estimated weight matrix, and $\hat{N}e$ is the estimated output of the RBF network used as a component of the controller. Then, the output voltage of the proposed controller is described in (16), and the structure of the controller is shown in Figure 4.

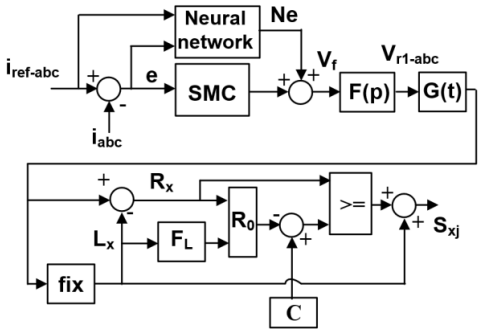

Fig. 4. Structure of the controller using NN.

IV. SIMULATION RESULTS AND DISCUSSION

The simulation system's parameters, along with the step changes in reference currents, are presented in Table II. There are 4 intervals of time, corresponding to 40 fundamental periods, each interval of 0.2 s with the reference peak current steps as 40 A, 30 A, 20 A, and 10 A respectively. The two method results are shown in Figures 5-12.

TABLE II. PARAMETERS OF THE SYSTEM

Description	Value
Voltage of the DC source	180 V
Angular frequency	100 π rad/s
Parameters of current controller *K*p, *K*i	0.1, 500
Load of each phase *R* and *L*	8.5 Ω and 5 mH
Frequency of carriers for POD f_c	3 kHz
Constant *C*	0.5
Constants α; β; γ; μ; *T*	3; 0.05; 0.05; 3.75×10^{5}; 3.97×10^{-5}

The method employing POD-PR provides the reference voltages in Figure 5(a) based on the reference currents, while the presented technique using ESMC offers those in Figure 5(b). The reference phase voltages of the two methods are zoomed in 0.16-0.2 s in Figures 6(a)-(b). Voltage waveforms have a significant difference in the ripples. The ripples in Figure 6(b) change in levels ±0.25 V and ±0.75 V, leading to the results in Figures (7)-(10).

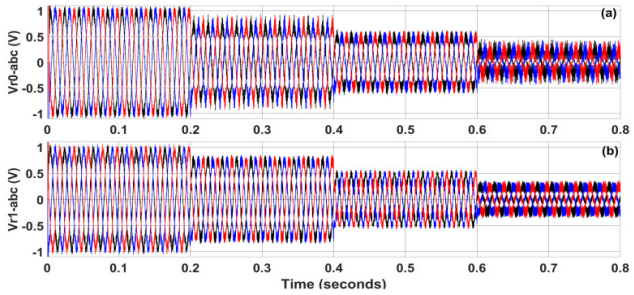

Fig. 5. Reference phase voltages: (a) POD-PR and (b) proposed method.

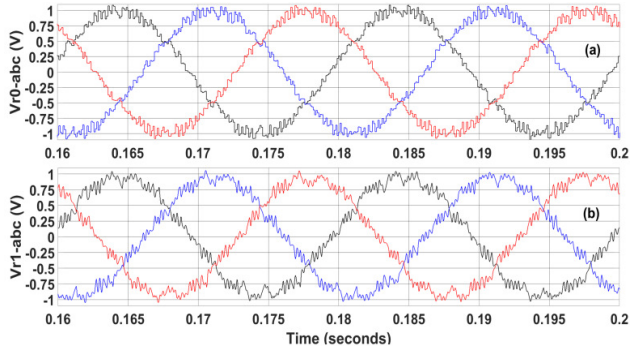

Fig. 6. Reference phase voltages zoomed in 0.16-0.2 s: (a) POD-PR and (b) proposed method.

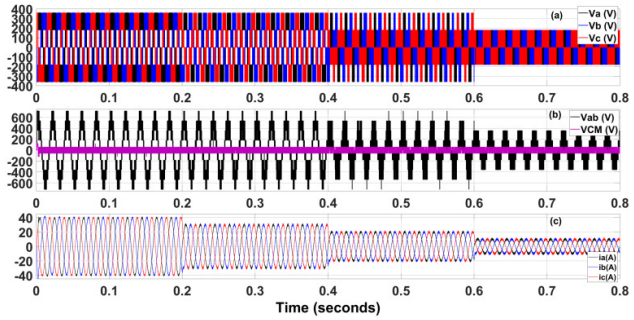

Fig. 7. Waveforms of POD-PR: (a) phase voltages, (b) phase-phase voltage and CMV, and (c) phase currents.

Normally, for multilevel 3-phase inverters, the voltage output of the inverter has only 3 phase wires and no neutral wire. Therefore, the phase-phase voltage quality should be considered and evaluated. The waveforms in Figure 7(b) show that the phase-phase voltage magnitude is up to $4\times V_{dc}$, as 720 V, in the three intervals from 0-0.6 s. This can also be clearly seen in Figure 9(b), while in Figure 8(b) of the proposed technique, it only exists in the first interval of 0-0.2 s. In the second and the third intervals, it is only $3\times V_{dc}$ and $2\times V_{dc}$, respectively. This can also be clearly seen in Figure 10(b).

The spectrum and THD value of the phase-phase voltage in Figure 11 are taken at the last period of every interval. The spectrum and THD value of the POD-PR method are illustrated in Figures 11(a)-(b), respective to the first interval and the last one. Similarly, those of the proposed technique are depicted in Figures 11(c)-(d). Those of the second and the third intervals also gave similar results. The THD values of the four intervals are summarized in Figure 12(a).

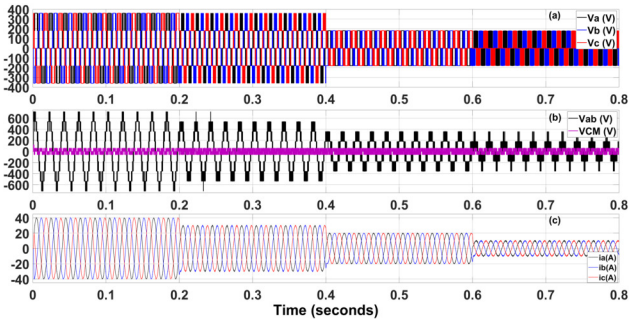

Fig. 8. Waveforms of ESMC: (a) phase voltages, (b) phase-phase voltage and CMV, and (c) phase currents.

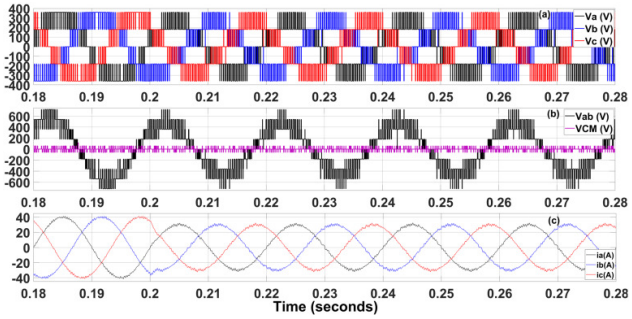

Fig. 9. Waveforms of POD-PR zoomed in 0.18-0.28 s: (a) phase voltage, (b) phase-phase voltage and CMV, and (c) phase currents.

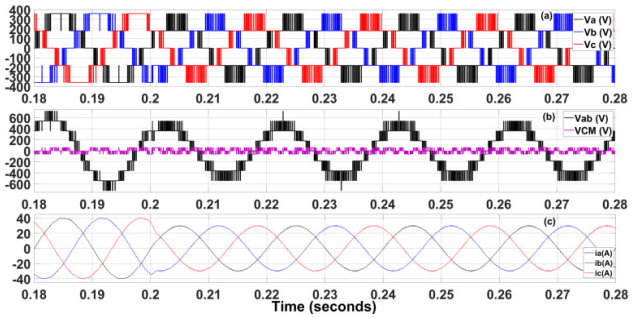

Fig. 10. Waveforms of the proposed technique zoomed in 0.18-0.28 s: (a) phase voltage, (b) phase-phase voltage and CMV, and (c) phase currents.

Although the phase-phase voltage of the POD-PR method has a level number greater than that of the proposed technique, its THD values are always higher than those of the technique suggested (Figures 11 and 12(a)). Its THD values are up to 26.88%, 40.29%, 65.03%, and 123.22%, respectively. On the other hand, those of the proposed technique are only 18.51%, 26.36%, 38.91%, and 80.95%, respectively.

Moreover, the highest individual harmonic magnitudes of the POD-PR method are up to 14% and 73%, respectively, in Figures 11(a)-(b) for the first (0-0.2 s) and the last interval (0.6-0.8 s), while those of the ESMC method are significantly low, only 4.84% and 23.3%, respectively (Figures 11(c)-(d)). This demonstrates the capability of the ESMC technique to distribute the spectrum across a broad range.

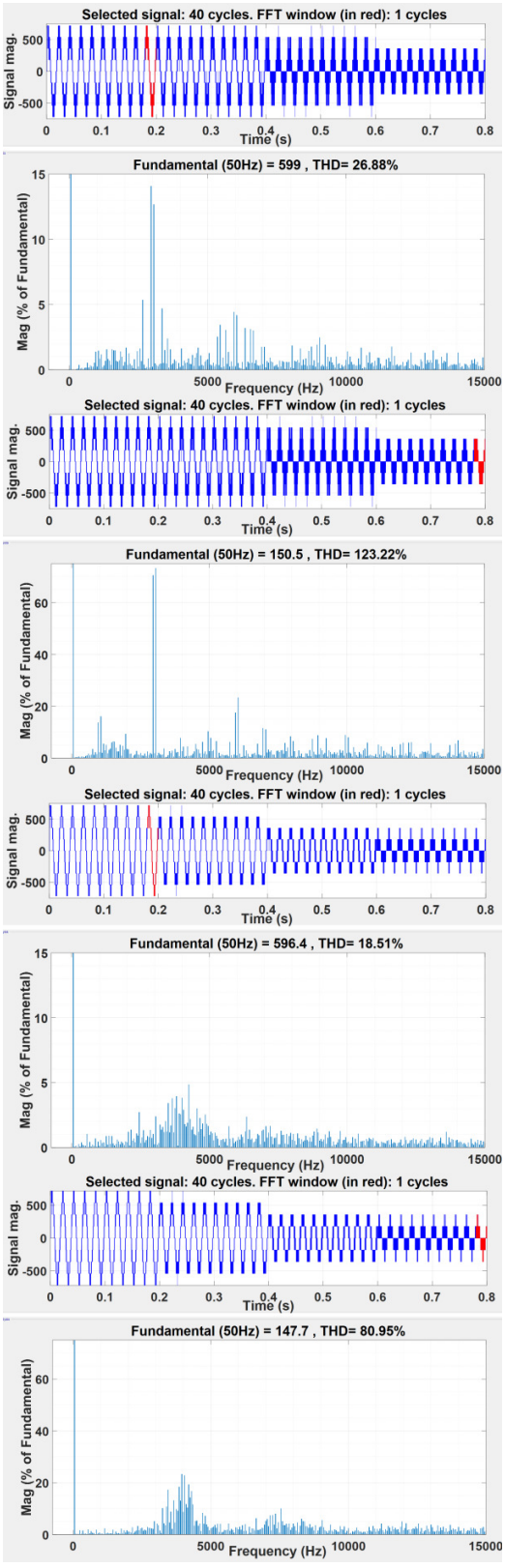

Fig. 11. Spectrum of phase-phase voltage: (a)-(b) POD-PR method and (c)-(d) proposed method.

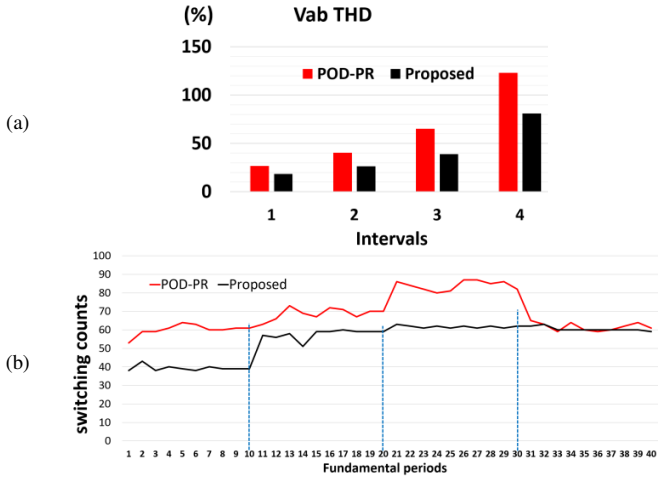

Fig. 12. (a) THD of phase-phase voltage and (b) switching count of each fundamental period.

In the entire time surveyed, from 0-0.8 s, there are 40 fundamental periods. The switching counts of the two methods in each 0.02 s period are presented in Figure 12(b). These results show that the switching counts of the proposed technique (Figure 12(b)) are always smaller than those of the POD-PR method, thus reducing the switching loss of the inverter.

V. CONCLUSION

This paper introduces a method for controlling three-phase MLIs using an enhanced sliding mode control technique based on neural networks, aimed at reducing the common mode voltage magnitude as achieved by the POD modulation. Additionally, this technique aids in decreasing the switching counts and minimizing voltage harmonics of MLIs. The proposed approach eliminates the need for carrier signals for modulation and PR current controllers, thereby streamlining hardware computations. Simulation results substantiate the efficacy of this method in a cascaded 5-level, 3-phase inverter system when compared to the conventional approach employing carriers of POD modulation and PR current controllers. Furthermore, the method's ability to distribute the spectrum over a wide range significantly diminishes the amplitudes of highest individual harmonics. This can help inverter to not need to use the passive filter at the output while power quality is guaranteed. In addition, this also lowers the acoustic noise to telecommunication and military equipment. In future research, this technique will be applied to reduce the current harmonics and the switching counts of MLIs of the grid-connected systems.

ACKNOWLEDGMENT

This work belongs to the project funded by Ho Chi Minh City University of Technology and Education, Vietnam.

REFERENCES

[1] K. Gudipati, H. V. R. Maramreddy, S. G. Kolli, V. A. Lakshmi, and G. S. Reddy, "Comparison of Pulse Width Modulation Techniques for Diode-Clamped and Cascaded Multilevel Inverters," *Engineering,*

Technology & Applied Science Research, vol. 13, no. 4, pp. 11078–11084, Aug. 2023, https://doi.org/10.48084/etasr.5939.

[2] W. Boucheriette, A. Moussi, R. Mechgoug, and H. Benguesmia, "A Multilevel Inverter for Grid-Connected Photovoltaic Systems Optimized by Genetic Algorithm," *Engineering, Technology & Applied Science Research*, vol. 13, no. 2, pp. 10249–10254, Apr. 2023, https://doi.org/10.48084/etasr.5558.

[3] M. J. Shah, K. S. Pandya, and P. Chauhan, "Direct ADC Controlled Asymmetric Cascaded Multilevel Inverter," *Engineering, Technology & Applied Science Research*, vol. 12, no. 4, pp. 9071–9077, Aug. 2022, https://doi.org/10.48084/etasr.5164.

[4] P. T. Giang, V. T. Ha, and V. H. Phuong, "Drive Control of a Permanent Magnet Synchronous Motor Fed by a Multi-level Inverter for Electric Vehicle Application," *Engineering, Technology & Applied Science Research*, vol. 12, no. 3, pp. 8658–8666, Jun. 2022, https://doi.org/10.48084/etasr.4935.

[5] V. T. Ha, P. T. Giang, and V. H. Phuong, "T-Type Multi-Inverter Application for Traction Motor Control," *Engineering, Technology & Applied Science Research*, vol. 12, no. 2, pp. 8321–8327, Apr. 2022, https://doi.org/10.48084/etasr.4776.

[6] A. Poorfakhraei, M. Narimani, and A. Emadi, "A Review of Modulation and Control Techniques for Multilevel Inverters in Traction Applications," *IEEE Access*, vol. 9, pp. 24187–24204, Feb. 2021, https://doi.org/10.1109/ACCESS.2021.3056612.

[7] V. Jayakumar, B. Chokkalingam, and J. L. Munda, "A Comprehensive Review on Space Vector Modulation Techniques for Neutral Point Clamped Multi-Level Inverters," *IEEE Access*, vol. 9, pp. 112104–112144, Jul. 2021, https://doi.org/10.1109/ACCESS.2021.3100346.

[8] D. Busse, J. Erdman, R. J. Kerkman, D. Schlegel, and G. Skibinski, "Bearing currents and their relationship to PWM drives," *IEEE Transactions on Power Electronics*, vol. 12, no. 2, pp. 243–252, Mar. 1997, https://doi.org/10.1109/63.558735.

[9] *Application Note, Motor Bearing Current Phenomenon, Rev: 08-08*. Yaskawa Electric America, Inc., 2008.

[10] C.-C. Hou, C.-C. Shih, P.-T. Cheng, and A. M. Hava, "Common-Mode Voltage Reduction Pulsewidth Modulation Techniques for Three-Phase Grid-Connected Converters," *IEEE Transactions on Power Electronics*, vol. 28, no. 4, pp. 1971–1979, Apr. 2013, https://doi.org/10.1109/TPEL.2012.2196712.

[11] M. A. Zdiri, B. Dhouib, Z. Alaas, F. B. Salem, and H. H. Abdallah, "Load Flow Analysis and the Impact of a Solar PV Generator in a Radial Distribution Network," *Engineering, Technology & Applied Science Research*, vol. 13, no. 1, pp. 10078–10085, Feb. 2023, https://doi.org/10.48084/etasr.5496.

[12] M. M. H. Milu, M. A. Rahman, M. A. Rashid, A. Kuwana, and H. Kobayashi, "Improvement of Classification Accuracy of Four-Class Voluntary-Imagery fNIRS Signals using Convolutional Neural Networks," *Engineering, Technology & Applied Science Research*, vol. 13, no. 2, pp. 10425–10431, Apr. 2023, https://doi.org/10.48084/etasr.5703.

[13] M. Kiruthika and S. Bindu, "Classification of Electrical Power System Conditions with Convolutional Neural Networks," *Engineering, Technology & Applied Science Research*, vol. 10, no. 3, pp. 5759–5768, Jun. 2020, https://doi.org/10.48084/etasr.3512.

[14] H.-G. Han, L. Zhang, Y. Hou, and J.-F. Qiao, "Nonlinear Model Predictive Control Based on a Self-Organizing Recurrent Neural Network," *IEEE Transactions on Neural Networks and Learning Systems*, vol. 27, no. 2, pp. 402–415, Oct. 2016, https://doi.org/10.1109/TNNLS.2015.2465174.

[15] B. Su, F. Zhang, and P. Huang, "Stability Analysis and RBF Neural Network Control of Second-Order Nonlinear Satellite System," *IEEE Transactions on Aerospace and Electronic Systems*, vol. 59, no. 4, pp. 4575–4589, Dec. 2023, https://doi.org/10.1109/TAES.2023.3243582.

[16] X. Shen, H. Wang, J. Li, Q. Su, and L. Gao, "Distributed Secondary Voltage Control of Islanded Microgrids Based on RBF-Neural-Network Sliding-Mode Technique," *IEEE Access*, vol. 7, pp. 65616–65623, 2019, https://doi.org/10.1109/ACCESS.2019.2915509.

[17] K. Ullah, J. Guzinski, and A. F. Mirza, "*Critical Review on Robust Speed Control Techniques for Permanent Magnet Synchronous Motor (PMSM) Speed Regulation*," *Energies*, vol. 15, no. 3, 2022, https://doi.org/10.3390/en15031235.

[18] H. R. Baghaee, A. K. Kaviani, M. Mirsalim, and G. B. Gharehpetian, "Harmonic optimization in single DC source multi-level inverters using RBF neural networks," in *2012 3rd Power Electronics and Drive Systems Technology (PEDSTC)*, Tehran, Iran, Oct. 2012, pp. 403–409, https://doi.org/10.1109/PEDSTC.2012.6183364.

[19] J. Gurram, N. S. Babu, and G. N. Srinivas, "Artificial neural network based DC-DC converter for grid connected transformerless PV system," *International Journal of Power Electronics and Drive Systems (IJPEDS)*, vol. 13, no. 2, pp. 1246–1254, Jun. 2022, https://doi.org/10.11591/ijpeds.v13.i2.pp1246-1254.

[20] H. Attia, "High performance PV system based on artificial neural network MPPT with PI controller for direct current water pump applications," *International Journal of Power Electronics and Drive Systems (IJPEDS)*, vol. 10, no. 3, pp. 1329–1338, Sep. 2019, https://doi.org/10.11591/ijpeds.v10.i3.pp1329-1338.

[21] J. Hou, D. Yao, F. Wu, J. Shen, and X. Chao, "Online Vehicle Velocity Prediction Using an Adaptive Radial Basis Function Neural Network," *IEEE Transactions on Vehicular Technology*, vol. 70, no. 4, pp. 3113–3122, Apr. 2021, https://doi.org/10.1109/TVT.2021.3063483.

[22] F. Yao, J. Zhao, X. Li, L. Mao, and K. Qu, "RBF Neural Network Based Virtual Synchronous Generator Control With Improved Frequency Stability," *IEEE Transactions on Industrial Informatics*, vol. 17, no. 6, pp. 4014–4024, Jun. 2021, https://doi.org/10.1109/TII.2020.3011810.

[23] S. Vijayalakshmi, V. Ganapathy, C. Anuradha, R. C. Ilambirai, and V. Ganesh, "Intelligent approach on sensorless control of permanent magnet synchronous generator," *International Journal of Power Electronics and Drive Systems (IJPEDS)*, vol. 13, no. 3, pp. 1770–1778, Sep. 2022, https://doi.org/10.11591/ijpeds.v13.i3.pp1770-1778.

[24] J. Fei, N. Liu, S. Hou, and Y. Fang, "Neural network complementary sliding mode current control of active power filter," *IEEE Access*, vol. 9, pp. 25681–25690, 2021, https://doi.org/10.1109/ACCESS.2021.3056224.

[25] Z. Laala, A. Benaissa, B. Rabhi, and M. F. Benkhoris, "Neural network controller for five phases shunt active power filter applied for five phase embarked electrical network," *International Journal of Power Electronics and Drive Systems (IJPEDS)*, vol. 14, no. 2, pp. 1024–1032, Jun. 2023, https://doi.org/10.11591/ijpeds.v14.i2.pp1024-1032.

[26] L. Abdelhak, B. Anas, B. Jamal, and E. O. Mostafa, "Optimized control of three-phase inverters to minimize total harmonic distortion in a grid-connected photovoltaic system," *International Journal of Power Electronics and Drive Systems (IJPEDS)*, vol. 13, no. 4, pp. 2255–2268, Dec. 2022, https://doi.org/10.11591/ijpeds.v13.i4.pp2255-2268.

[27] V. Q. Vinh and V. T. Ha, "Improved Torque Ripple of Switched Reluctance Motors using Sliding Mode Control for Electric Vehicles," *Engineering, Technology & Applied Science Research*, vol. 13, no. 1, pp. 10140–10144, Feb. 2023, https://doi.org/10.48084/etasr.5559.

[28] M. S. Shah, T. Mahmood, A. U. Rehman, M. Q. Manan, and M. F. Ullah, "Power Quality Improvement using Dynamic Voltage Restorer with Real Twisting Sliding Mode Control," *Engineering, Technology & Applied Science Research*, vol. 12, no. 2, pp. 8300–8305, Apr. 2022, https://doi.org/10.48084/etasr.4734.

[29] A. Maafa, H. Mellah, K. Ghedamsi, and D. Aouzellag, "Improvement of Sliding Mode Control Strategy Founded on Cascaded Doubly Fed Induction Generator Powered by a Matrix Converter," *Engineering, Technology & Applied Science Research*, vol. 12, no. 5, pp. 9217–9223, Oct. 2022, https://doi.org/10.48084/etasr.5166.

[30] Q.-T. Tran and V.-Q. Nguyen, "Reduction of common mode voltage for grid-connected multilevel inverters using fuzzy logic controller," *International Journal of Power Electronics and Drive Systems (IJPEDS)*, vol. 14, no. 2, pp. 698–707, Jun. 2023, https://doi.org/10.11591/ijpeds.v14.i2.pp698-707.